Journal of

Applied and Computational Mechanics

Shahid Chamran
University of Ahvaz

Journal of Applied and Computational Mechanics

Research Paper

Mixed Convection Heat Transfer and Entropy Generation in a Water-filled Square Cavity Partially Heated from Below: The Effects of Richardson and Prandtl Numbers

Nawal Ferroudj[1,2] [ID], Hasan Koten[3] [ID], Saadoun Boudebous[4] [ID]

[1] Faculty of Process Engineering, University of Salah Boubnider Constantine 3, 25016, Algeria, Email: n.ferroudj@ensbiotech.edu.dz

[2] Laboratory of Biotechnology, National Higher School of Biotechnology (ENSB), Constantine 3, Algeria ,25016, Email: n.ferroudj@ensbiotech.edu.dz

[3] Mechanical Engineering Department, Computational Fluid Dynamics Laboratory, Istanbul Medeniyet University, Turkey, Email: hasan.koten@medeniyet.edu.tr

[4] Faculty of Sciences and Applied Sciences, University of Larbi BenM'hidi, Oum el Bouaghi, 04000 , Algeria, Email: s.boudebous@gmail.com

Abstract. In the present study, fluid flow, heat transfer, and entropy generation for mixed convection inside a water-filled square cavity were investigated numerically. The sidewalls of the cavity, which move upwards, are kept at low-temperature T_c while only a part in the center of the bottom wall is kept at high-temperature T_h and the remaining parts are kept adiabatic. The governing equations, in stream function–vorticity form, are discretized and solved using the finite difference method. Particular attention was paid to the influence of the Prandtl numbers of 5.534, 3.045 and 2, corresponding respectively to the water temperatures of 303.15 K, 333.15 K and 363.15 K. The numerical results are presented in the form of streamlines, isotherms, and entropy generation contours for different values of the Richardson numbers at an arbitrary Reynolds number Re=10^2. Besides this, the evolution of the average Nusselt number and the average entropy generation is also reported. The obtained results show interesting behaviors of the flow and thermal fields, which mainly involve stable symmetric and non-symmetric steady-state solutions, as well as unsteady regimes, depending on specific values of the Richardson and Prandtl numbers. It is additionally observed that the average Nusselt number increases and the average entropy generation decreases when both the Richardson and Prandtl numbers increase.

Keywords: Mixed convection, Entropy generation, Finite difference method, Prandtl number, Richardson number, Nusselt Number.

1. Introduction

Flows involving both forced and natural convection, commonly referred to as mixed convection, are very often encountered in many industrial applications as evidenced, for example, by several recently published papers concerning electronic cooling [1, 2], air conditioning [3, 4], thermal design of building [5], solar collectors [6], chemical processing equipment [7], heat exchangers [8]. In recent years, convective fluid flows, in different enclosures, using the suspension of the Nano-Encapsulated Phase Change Materials (NEPCMs) have created a new research area and opened up radically new opportunities for many industrial applications. The following articles [9-12] have made a substantial contribution to the understanding of this phenomenon and, the obtained results show that the presence of NEPCM particles improves effectively the heat transfer.

All real fluids in motion in a process that involve heat and/or mass transfer result in significant energy losses generally referred to as the "entropy generation". This phenomenon arises due to the velocity, thermal and/or solutal gradients. The theory and the computation of the entropy generation was introduced for the first time by Bejan and reported in several of his works, e.g. [13, 14]. Numerous studies have been carried out to understand the fluid flow and heat transfer process in closed cavities in mixed convection regime. Most of the important published works that examine the heat transfer process by mixed convection in enclosures with different shapes that integrated non-Newtonian fluids and nanofluids were reported more recently in the review articles by Izadi et al.[15], Mustafa Abdul Salam et al. [16] and, Yang and Kai Du [17].

Entropy generation in mixed and natural convection has been the focus of research by numerous investigators as reviewed by Oztop and Al-Salem [18] Sciacovelli et al.[19] and, Biswal and Basak [20]. Since then, many other numerical studies in the same area have been carried out and, by focusing solely over the last two years some of them can be described here. Sheikholeslami et al. [21] investigated, by applying a novel numerical simulation approach based on the Finite Element Method FEM, entropy generation of a nanomaterial flow in the presence of Lorenz forces within a porous enclosure. They showed that increasing permeability makes the Bejan number decline, boundary layer thickness enhances with a rise of Lorentz force. In addition, two precise formulas were suggested for the estimation of the Bejan number and average Nusselt number. Sheikholeslami et al. [22]

scrutinized entropy generation of nanomaterial through a quad-lobed tube equipped with single or dual helical tape. One of their findings is that a greater value of the revolution of tape (N) leads to a reduction in thermal entropy generation ($S_{gen,th}$) about 0.48% when the number of tapes (TTn) =2 and Re=20,000, while viscous entropy generation ($S_{gen,f}$) experiences 35.58% augmentation with rising of the number of tapes (TTn) when N=4, Re=400. The effects of a partial elastic wall, an inclined magnetic field, and a rotating circular cylinder on the entropy generation of convective heat transfer of carbon nanotube (CNT)–water nanofluid filled U-shaped cavity was carried out by Selimefendigil et al. [23]. They demonstrate that the entropy generation rates with varying Hartmann (Ha) number, rotational velocity, and location of the cylinder are different for the left and right parts of the domains while impacts of elastic wall properties on the entropy generation rate are slight. Rabbi et al. [24] examined magneto-hydrodynamic convection and entropy generation within a square tank occupied with Cu-H_2O nanomaterial. The numerical method based on the Galerkin residual finite element analysis has been implemented and, the Artificial Neural Network (ANN) model was used as an advanced predictive tool. The investigation has been done for Hartmann number (Ha 0 – 100), Rayleigh number (Ra 10^3-10^7), and nanomaterial concentration (φ 0 – 0.05). Streamlines, isotherm contours, and entropy generation contours are discussed thoroughly. It has been shown that the existence of external Lorentz forces affects both the Nusselt (Nu) and the Bejan (Be) numbers. In addition, the impact of Ha and φ on Nu and Be found from the numerical heat transfer analysis has been predicted and compared with ANN prediction model. Monda et al. [25] numerically analyzed MHD mixed convection flow, and entropy generation of AL_2O_3-water nanofluid flowing in a lid-driven trapezoidal enclosure. The stream-function vorticity formulation is used to solve the discretized coupled non-linear partial differential equations by a finite differences method. The obtained results show significant changes in streamlines, temperature, concentration and, global entropy generation contours for high Richardson number. Ebrahimi et al. [26] conducted the computational modeling of laminar mixed convection heat transfer of nanofluids inside a closed elbow-shaped cavity (CESC), using a finite volume method. Nusselt number, friction coefficient, dimensionless velocity in different sections of the cavity, temperature and entropy generation contours are presented. They argue that increasing the Grashof number implies an improvement in the fluid circulation mechanism, which results in a substantial reduction in the generation of entropy in the studied geometry. In addition, in the lower areas of the hot surface, entropy generation is always the least. Khosravi et al. [27] utilized Fluent software and an Artificial Neural Network model (ANN) in order to estimate the entropy generation of graphene–platinum/water hybrid nanofluid flow to assess how a new cylindrical microchannel heat sink with wavy-shaped fins performs. A variety of Reynolds numbers, nanoparticle concentrations as well as wave amplitudes is used to simulate the problem, while the heat flux is constant. They concluded therefore that increasing each factor, including wave amplitude, particle fraction, and Reynolds number, causes a decline in the thermal entropy generation rate, while frictional entropy rises significantly. The Bejan number was obtained greater than 0.98 in all cases, which means that irreversibility mainly results from the thermal entropy generation. Cimpean and Pop [28] investigated entropy generation in an inclined square cavity filled with a porous media saturated by a nanofluid with sinusoidal temperature distribution on the side walls, adiabatic conditions on the upper wall and a heat source at the lower wall. The governing equations and the entropy generation, in terms of the dimensionless variables, are discretized and solved by a finite difference method of second-order accuracy. The authors conclude that the conditions of the model and the values of the studied parameters have a significant effect on the existence of the irreversibility phenomena.

Relatively low number of numerical investigations are performed in mixed convection for various configurations which include the effect Prandtl number. In this context, Maougal and Bessaih [29] performed a numerical investigation on the entropy generation in mixed convection in a square cavity, filled with a saturated porous medium and heated by a discrete set of heat sources. Simulations were carried out for Reynolds number Re=20, 40, 80, 100, 200, Darcy number, Da=10^{-5}-10^{-1}, Prandtl number, Pr=0.015, 0.7, 10, 10^3, and aspect ratio, D/H =0.05, 0.10, 0.15, 0.2, 0.25. Their results showed that the Reynolds and Prandtl numbers have the same effect on the entropy production and, their increase improves the heat transfer. Roy et al. [30, 31, 32] investigated the effect of the Prandtl on entropy generation during the mixed convection in a square cavity where the bottom wall is isothermally hot, sidewalls are cold, and the top wall is adiabatic. Simulations have been carried out for Prandtl number Pr= 0.026 and 7.2, the Reynolds number Re varies between 10 and 100, and Grashof number Gr varies between 10^3 and 10^5. In [30] the effect of moving horizontal or vertical wall(s) is considered, in [31] the effect of various thermal boundary conditions is studied. in [32], the cavity is filled with a porous medium and the effect of thermal boundary condition is reported. More recently, Roy et al. [33] delt with the same problem as those described above but in porous triangular cavities. In each considered investigation, these authors report the values of the parameters that contribute to minimize the entropy generation. However, the topic in question continues to receive interest as evidenced in the papers recently published by Bhatti et al. [34, 35], Khan et al. [36], Ögüt [37], Mehta and Pati [38], and Kashyap et al. [39]. Bhatti et al. [34] investigated entropy generation during heat and mass transfer in peristaltic Ellis fluid flow through a nonuniform channel. Mathematical and graphical analyses of the velocity profile, temperature profile, concentration profile, and entropy profile are presented for the Schmidt, Eckert, Soret, Prandtl, and Brinkmann numbers, compliant wall parameters, and Ellis fluid parameters. Bhatti et al. [35] examined the entropy generation on the interaction of nanoparticles over a stretching porous sheet with nonlinear thermal radiation. Simultaneous effects of the porous medium, Radiation parameter, nanoparticle volume fraction, Prandtl number, Brinkman number, and Reynolds number are demonstrated through graphs. Khan et al. [36] analyzed numerically the entropy generation in an incompressible thermal flow of Newtonian fluids over a thin needle that is moving in a parallel stream. Water and air are considered working fluids. The effects of Prandtl number, Eckert number, and dimensionless temperature parameter are discussed graphically in detail. It is shown that entropy generated due to heat transfer and fluid friction in water is more than in air. Ögüt [37] studied the entropy generation in laminar mixed convection in an inclined square lid-driven enclosure in the presence of magnetic field. The principal parameters considered in this study are : Richardson number (from 0.01 to 100), Prandtl number (from 0.1 to 1.0), inclination angle of enclosure (from 0° to 180°), Hartmann number (from 0 to 100) and magnetic field direction (0°). It was found that the inclination angle of enclosure is an effective parameter on entropy generation especially for higher Richardson number (Ri > 1) due to domination of natural convection. However, Hartmann number is effective on both heat transfer and entropy generation for all values of Richardson and Prandtl numbers and it decreases the convective fluid flow and entropy generation. Mehta and Pati [38] discussed the thermo-fluidic and entropy generation characteristics for laminar forced convective flow through wavy channel at different Prandtl numbers. Results are presented for the following range of parameters: Reynolds number (Re), Prandtl number (Pr), dimensionless amplitude (α) and, dimensionless wavelength (λ) which vary from 5 to 200, 0.72 to 100, 0.3 to 0.7, and 0.5 to 1.5 respectively. They observed that the thermal entropy generation contribution is higher than the viscous one for all the cases considered, the local thermal entropy generation distribution varies with the Re, Pr, and geometrical configuration of the channel and, for a smaller amplitude (α = 0.3) the total entropy generation is minimum in the considered range of Re and Pr. More recently, Kashyap et al. [39] investigated the effects of three different Prandtl number fluids (Pr = 0.025, 5.83 and 151) on convective heat transfer inside a closed square cavity with an adiabatic left wall and three other cold walls. A centrally positioned square hot block with respective blockage ratios of 0.25 and 0.5 heats the cavity. One of their conclusions is that the total entropy generation in mixed convection, the heat transfer irreversibility mostly dominates the entropy generation at all Pr irrespective of Ri values as indicated by large average Bejan number.
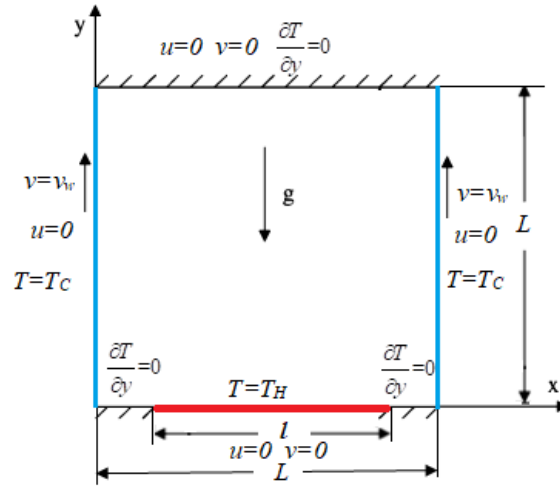
Fig. 1. Physical model and boundary conditions

From this literature review, it appears that the numerical studies of mixed convection in confined spaces taking into account the impact of Richardson and Prandtl numbers on the entropy generation are relatively scarce. On the other hand, all authors use different fluids to examine the impact of this number when studying convective flows. For our part we have opted for a new approach which consists in considering the same fluid at different temperatures, i.e. at different Prandtl numbers. For this purpose, we chose water as the working fluid, because of its many practical applications in engineering [40] and on the other hand, in contrast to other fluids, it offers a significant disparity in the value of the Prandtl number depending on the temperature. Indeed, its value ranges from 11.44 and 0.9996 for temperatures from 5°C to 100°C respectively.

2. Physical Model and Mathematical Formulation

2.1 Physical model

The schematic diagram of the two-dimensional square cavity of side length L considered in the present study is highlighted in Fig. 1. The lateral walls are maintained at a constant cold temperature T_C and move upwards with a constant velocity v_w. A heat source of size $l = 0.8$ L is located at the center of the bottom wall of the cavity and maintained at a constant high temperature T_H. All remaining parts of the cavity are considered adiabatic. The mechanism for moving the side walls is illustrated in the article by Roy et al. [30].

2.2 Mathematical formulation

The governing equations for the present problem for steady two-dimensional mixed convection flow in a square cavity are the conservation continuity of mass, momentum and energy equation that can be expressed as follows [41] :

- Continuity equation :

$$\frac{\partial u}{\partial x} + \frac{\partial v}{\partial y} = 0 \tag{1}$$

- x momentum equation :

$$\frac{\partial u}{\partial t} + u\frac{\partial u}{\partial x} + v\frac{\partial u}{\partial y} = -\frac{1}{\rho}\frac{\partial P^*}{\partial x} + \frac{\mu}{\rho}\left(\frac{\partial^2 u}{\partial x^2} + \frac{\partial^2 u}{\partial y^2}\right) \tag{2}$$

- y momentum equation :

$$\frac{\partial v}{\partial t} + u\frac{\partial v}{\partial x} + v\frac{\partial v}{\partial y} = -\frac{1}{\rho}\frac{\partial P^*}{\partial y} + \frac{\mu}{\rho}\left(\frac{\partial^2 v}{\partial x^2} + \frac{\partial^2 v}{\partial y^2}\right) + g\beta(T - T_c) \tag{3}$$

- Energy equation :

$$\frac{\partial T}{\partial t} + u\frac{\partial T}{\partial x} + v\frac{\partial T}{\partial y} = \alpha\left(\frac{\partial^2 T}{\partial x^2} + \frac{\partial^2 T}{\partial y^2}\right) \tag{4}$$

The flow is unsteady, laminar and incompressible. All other properties of the fluid are assumed constant, except for the density of the fluid that generates the buoyancy forces, in accordance with Boussinesq's approximation. Taking into account these assumptions, the momentum governing equations can be given as follows in the vorticity-stream function formulation [41]:

- Vorticity equation :

$$\frac{\partial \omega}{\partial t} + u\frac{\partial \omega}{\partial x} + v\frac{\partial \omega}{\partial y} = \frac{\mu}{\rho}\left(\frac{\partial^2 \omega}{\partial x^2} + \frac{\partial^2 \omega}{\partial y^2}\right) + g\beta\frac{\partial T}{\partial x} \tag{5}$$

- Stream function equation :

$$\frac{\partial^2 \psi}{\partial x^2} + \frac{\partial^2 \psi}{\partial y^2} = -\omega \tag{6}$$

The vorticity is defined as: $\omega = \partial v / \partial x - \partial u / \partial y$ and the velocity components in the x and y directions, respectively are:

$$u = \frac{\partial \psi}{\partial y}, \ v = -\frac{\partial \psi}{\partial x} \tag{7}$$

2.3 Initial and boundary conditions

Numerical solution of the previous equations is based on the following initial and boundary conditions:

- Initial conditions: (t = 0) :

$$0 \leq y \leq L \quad \& \quad 0 \leq x \leq L \quad T = T_C \quad \& \quad \psi = \omega = 0 \tag{8a}$$

- Boundary conditions (t > 0) :

$$\left.\begin{array}{c} x = 0 \\ x = L \end{array}\right\} \quad \& \quad 0 \leq y \leq L; \quad u = \psi = 0; \quad v = v_w = \frac{\mu}{\rho L} Re; \quad T = T_C \tag{8b}$$

$$y = 0 \quad \& \quad 0 \leq x \leq (L-l)/2 \quad \& \quad (L+l)/2 \leq x \leq L \quad u = v = \psi = \frac{\partial T}{\partial y} = 0 \tag{8c}$$

$$y = 0 \quad \& \quad (L-l)/2 \leq x \leq (L+l)/2 \quad u = v = \psi = 0 \quad \& \quad T = T_H \tag{8d}$$

$$y = L \quad \& \quad 0 \leq x \leq L \quad u = v = \psi = \frac{\partial T}{\partial y} = 0 \tag{8e}$$

2.4 Nusselt number

Local and average Nusselt numbers has been computed for the heated part of the bottom wall of the cavity and are determined from the following expression:

$$Nu_{loc} = -\frac{1}{\Delta T} \frac{\partial T}{\partial y}\bigg|_{y=0} \qquad \overline{Nu} = \frac{1}{l} \int_{(L-l)/2}^{(L+l)/2} Nu_{loc} dx \tag{9}$$

2.5 Entropy generation

The local entropy generation is given by [42] :

$$s_{gen} = \underbrace{\frac{k}{T_0^2}\left[\left(\frac{\partial T}{\partial x}\right)^2 + \left(\frac{\partial T}{\partial y}\right)^2\right]}_{S_{th}} + \underbrace{\frac{\mu}{T_0}\left[2\left(\frac{\partial u}{\partial x}\right)^2 + 2\left(\frac{\partial v}{\partial y}\right)^2 + \left(\frac{\partial u}{\partial y} + \frac{\partial v}{\partial x}\right)^2\right]}_{S_{ff}} \tag{10}$$

where S_{th} is the entropy that is generated due to the thermal irreversibility (heat transfer) and S_{ff} is the entropy that is generated due to the flow irreversibility (fluid friction).

The total entropy generation is the integral over the system volume of the local entropy generation:

$$\overline{s_{gen}} = \frac{1}{L^2} \int_0^L \left\{ \int_0^L s_{gen} dx \right\} dy \tag{11}$$

2.6 Bejan number

The local Bejan number is a dimensionless number that provides a measure of the importance of the thermal entropy generation compared to the total entropy generation. It is expressed by:

$$Be = \frac{S_{th}}{S_{th} + S_{ff}} \tag{12}$$

Also, the average Bejan number is given by:

$$\overline{Be} = \frac{1}{L^2} \int_0^L \left\{ \int_0^L Be \ dx \right\} dy \tag{13}$$

During the numerical modeling of mixed convection, some parameters should be chosen to serve as a comparison with the overwhelming majority of studies reported These include, among others, the Richardson number (Ri) which characterizes the flow regime and provides a measure of the influence of free convection in comparison with forced convection, the Prandtl number (Pr), which is being designated as the ratio of the momentum diffusivity to the thermal diffusivity, and the Reynolds number (Re) used to represent the ratio of inertial forces to viscous forces. These different numbers are defined respectively by the following relationships:

$$Ri = \frac{Gr}{Re^2} \quad Pr = \frac{\nu}{\alpha} \quad Re = \frac{v_w L}{\nu}$$

where Gr is the Grashof number, $Gr = g\beta\Delta T L^3 / \nu^2$, $\Delta T = T_H - T_C$ is the temperature difference and v_w is the side wall velocity.

3. Numerical Procedure and Validation

3.1 Numerical procedure

The finite difference method is used to solve the governing equations (4)-(7) with the corresponding boundary conditions, Eqs. (8a-8e). Temporal discretization has been achieved using the Alternating Direction Implicit (ADI) method. More details on this procedure can be found in Micula and Pop [43]. High-resolution spatial scheme was used for all equations. Convective terms in Eqs. (4, 5) have been discretized into a third-order upwind scheme as proposed by Kawamura et al. [44]. Diffusive terms, as well as the terms including the first derivatives, have been discretized by a fourth-order accurate scheme. An iterative procedure based on the successive Non Linear Over Relaxation method (NLOR) was used to solve the discretized stream function equation Eq. (6). In addition, once the velocity and temperature fields obtained we can then determine the characteristics of the entropy generation (Eqs.10, 11, 12), the average Nusselt number along the hot part of the bottom wall (Eq. 9), and the average Bejan number (Eq. 13). An in-house FORTRAN code, with a double precision accuracy, has been developed for solving the mathematical model under consideration.

It was also clearly established, (see for example Bejan [45]) that the equation describing the entropy generation depends strongly, not only on the thermo-physical properties of the working fluid but also on a reference temperature (T_0). For this purpose, the reference values of the thermo-physical properties of water at 30°C (303.15 K), 60°C (333.15 K) and, 90°C (363.15 K) listed in Table 1, are from Dinçer and Zamfirescu [46] and, Fig.2 shows the variation of the Prandtl number (Pr) as a function of temperature. Furthermore, the Reynolds number (Re) and the temperature difference ΔT are kept constant at 10^2, and 2 K respectively. On this point, and as indicated by Ferziger and Peric [47] the use of the Boussinesq approximation in the Navier-Stokes equations introduces errors of the order of 1% if the temperature differences are less than 2°C for water. In addition, Pallares et al. [48] state that, at Ra=1.2 10^5 (ΔT=4.6 °C), physical properties of water have a variation of about 9% and non-Boussinesq effects begin to be important. On the other hand, the length L of the cavity was considered as the typical reference length of the system geometry of the study and will be used to compute the values of the non-dimensional parameters mentioned above. In view of this, it was deemed appropriate to immediately fix the ideas on the variation of the Richardson number (Ri) as a function of the length (L) of the cavity that we have presented in Fig. 3, so as to see precisely the specific value of Ri that would correspond more truly to L for each of the considered Prandtl numbers (Pr). The proposal has been suggested previously by Goodarzi et al. [49], and very recently by Patil et al. [50], that have dealt with the investigation of entropy generation due to fluid flows in the mixed convection regime.

To achieve clarity in order to facilitate understanding of the adopted numerical procedure, the main steps are described below:

1. Specification of the thermophysical properties of the working fluid.

Once the fluid and its temperature (To) have been selected, we can access all of its other thermophysical properties (ρ, μ, α, k, β and, Pr) from table 1. Note that these thermophysical properties of the working fluid may be changed depending on the temperature To.

2. Specification of the boundary conditions.

For this, we need to set a temperature difference (ΔT=2K), the length of the cavity (L), and the Reynolds number (Re=100). We then get the low-temperature T_C, the high-temperature T_H and, the sidewall velocity v_w as follows:

$$T_C = T_o - \frac{\Delta T}{2}; \quad T_H = T_o + \frac{\Delta T}{2}; \quad v_w = \frac{\mu}{\rho L} Re$$

Here too, these boundary conditions can be changed depending on the temperature To (i.e. Prandtl number) and the length of the cavity (L).

1. Numerical resolution.

The equations (4, 5, 6 and 7) are used to determine the dynamic and thermal fields, while equation (10) the entropy generation.

2. Computation of the non-dimensional parameters.

The Richardson number (Ri) is identified as the primary control parameter in this study. It is given by the following equation:

$$Ri = \frac{Gr}{Re^2}$$

where Gr is the Grashof number $Gr = g\beta\Delta T L^3 / \nu^2$.

As a final point, it must be noted that all parameters are known to calculate these dimensionless numbers. These different steps are carried out for each length of the cavity L (i.e. each Richardson number) and then after, for each Prandtl number.

Table 1. Thermo-physical properties of pure water at atmospheric pressure [46].

To (°C)	ρ (kg m⁻³)	μ (kg m⁻¹ s⁻¹)	α (m² s⁻¹)	k (W m⁻¹ K⁻¹)	β (K⁻¹)	Pr
30	995.7	7.977 10^{-4}	1.4477 10^{-7}	6.03 10^{-1}	3.051 10^{-4}	5.534
60	983.2	4.666 10^{-4}	1.5585 10^{-7}	6.41 10^{-1}	5.221 10^{-4}	3.045
90	965.3	3.145 10^{-4}	1.62903 10^{-7}	6.613 10^{-1}	6.958 10^{-4}	2.000

Table 2. Grid independence test: average Nusselt number and total entropy generation for Ri=0.48 and Pr = 5.534

Grid	$\overline{Nu}$	Relative error %	$\overline{S_{gen}}$	Relative error %
41x41	11.1964	6.20	4.1762	5.03
81x81	11.8402	0.84	4.0265	1.26
101x101	11.8814	0.49	3.9898	0.35
161x161	11.9259	0.12	3.9758	0.02
201x201	11.9399	-----	3.9763	-----

3.2 Grid independency test

Numerical tests have been made to ensure the accuracy of results for the grid used in this study. Five grid sizes (41x41; 81x81; 101x101, 161x161 and 201x201) have been considered. These numerical tests are carried out for the case of Reynolds number Re=100, Prandtl number Pr=5.534 (Water at 303K) and Richardson number Ri =0.48. Table 2 shows the convergence of the average Nusselt number and the total entropy generation. It should be noted that the maximum relative error does not exceed 1% between the grid sizes of 101×101, and 161x161 compared to the grid size of 201×201. Therefore, it was decided to use a non-uniform grid with 101×101 grid points for all calculations allowing a balance between accuracy and CPU time.

3.3 Code validation

First validation tests of the natural convection in a square cavity heated from below and cooled from others at Ra=10^5 and Pr=0.71 have been verified. The streamlines and isothermal lines are compared with those of Asad et al. [51], and Jani et al. [52] (Fig. 4). It is observed qualitatively, that the results agree with the earlier works.

The code is also tested while considering the same problem in the same geometrical configuration, but this time the comparison is related to the vertical velocity component along the horizontal centerline of cavity obtained by Jani et al. [52] and that achieved by the present code (Fig. 5). We therefore note that quantitatively the results are in good agreement.

Once again, the code was tested considering the work of Aydin and Yang [53] which deals with a numerical study of mixed convection in a cavity having a locally heated bottom wall and cold descending sidewalls. The dimensionless velocity components V=v/v_w along the horizontal centerline (Y=0.5), predicted by Aydin and Yang [53] for different Richardson numbers at ε=l/L=1/5 and the present work, are shown in Fig. 6. A comparison of the results demonstrates good agreement.
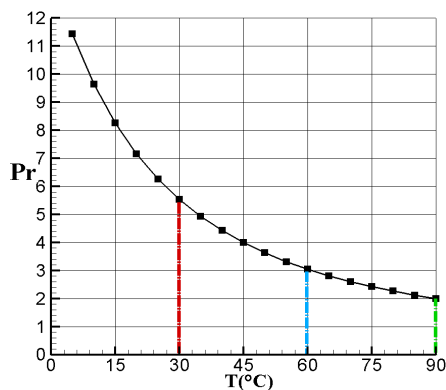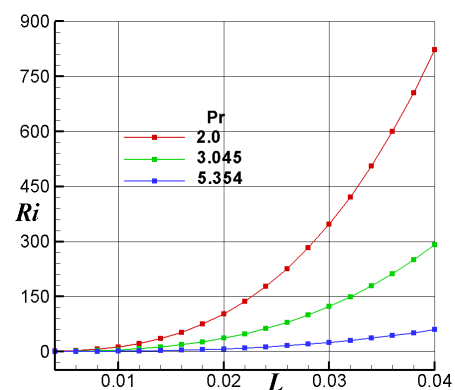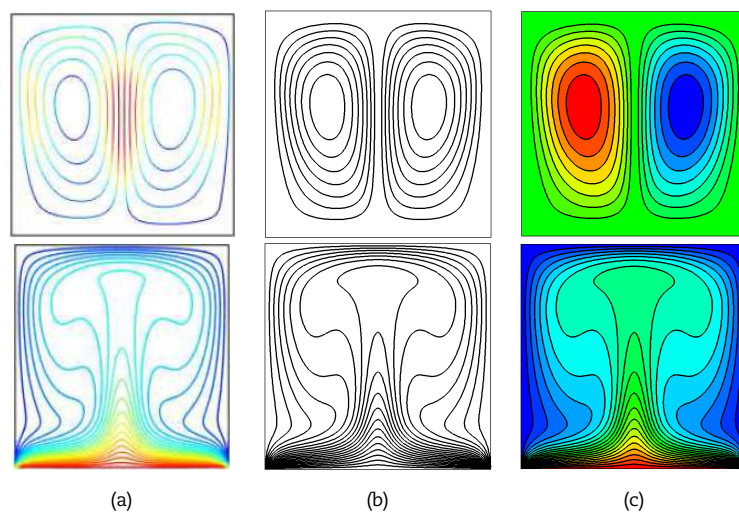

Fig. 2. Water Prandtl number versus Temperature [46]

Fig. 3. Variation of Ri as a function of L

(a)	(b)	(c)

Fig. 4. Comparison of the streamlines (upper row) and isotherms (bottom row) between numerical results by (a) Asad et al. [51], (b) Jani et al.[52] and (c) present work, at Ra=10^5 and Pr=0.71
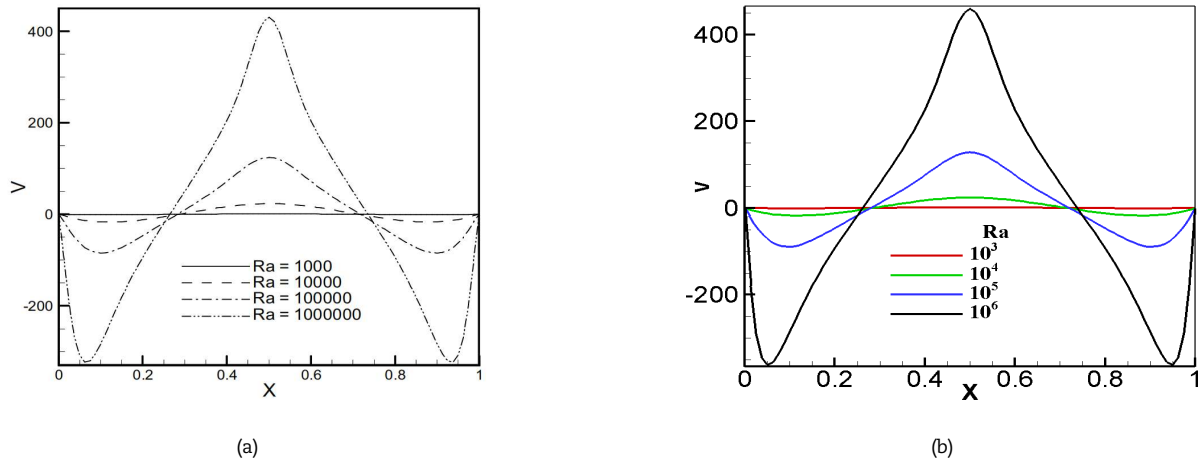
(a)   (b)

Fig. 5. Comparison of the vertical velocity component along the horizontal centerline of cavity, (a) Jani et al. [52] and (b) present work, at different Ra and Pr=0.71
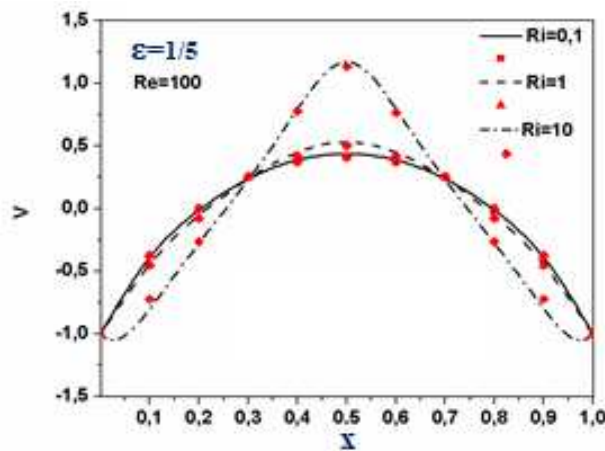

Fig. 6. Comparison of the vertical velocity component along the horizontal centerline of the cavity for Ri=0.1, 1. And 10 at Pr=0.71. Lines present work and, symbols: Aydin And Yang [53]

4. Results and Discussion

In this section, we investigate and discuss the scope of the effects of the Prandtl number on water flow, heat transfer, and entropy generation for different values of the governing parameters. The Richardson number, which is computed based on the thermophysical properties of water and the length L of the cavity is identified as the primary control parameter for heat and fluid flow inside the cavity. Furthermore, despite the fact that the numerical solution implies a time-dependent solution, it should be noted that only results about stable fluid flows are shown here.

4.1 Dynamic and thermal fields

The determination of the entropy generation depends on the velocity and temperature gradients, that is why the dynamic and thermal fields need to be examined in the first instance. The structure of streamlines and isotherms presented in Fig. 7 (a), (b) and, (c) for the values of the Prandtl number of 2., 3.045, and 5.534 respectively, show that the fluid circulation inside the cavity depends strongly on the Richardson number (i.e. the length of the cavity). One must nevertheless note that each figure presents the cavity with its own dimension measured on the x, y, axis. The results of the various numerical simulations show the existence of three very distinct types of flows according to the value of this parameter. The first type occurs at low values of Ri. The streamlines are characterized by the presence, inside the cavity, of two strictly symmetric cells with respect to the vertical axis passing through the middle of the cavity (first column of Fig. 7 a,b,c). The one on the left turns clockwise and the one on the right turns counterclockwise. Forces due to the movement of the side walls are large enough to draw heat from the heated portion, located on the bottom wall of the cavity, to evenly distribute it along these walls. The second type occurs as the Richardson number exceeds a critical value (first bifurcation). In this particular case, unsymmetrical flow structures and temperature distributions are observed inside the enclosure (second column of Fig. 7 a,b,c). The third and last type takes place when the Richardson number continues to increase in order to exceed a second critical value (second bifurcation). Noticeable and meaningful changes in streamlines and isotherms are observed (third column of Fig. 7 a, b ,c). In this case, the flow is predominantly composed of four symmetric cells, two counter-rotating cells located in the center of the cavity due to buoyancy forces, and the other two, also counter-rotating due to viscous forces, are weak and adjacent to the lateral sidewalls. Inside each of them, two minor vortices appear at the bottom and top corners. In this instance, all the heat from the hot source is propagated through the center of the cavity. It should be noted, however, that if the flow changes from a steady state to chaos the increase of Richardson number shall be stopped. It's a similar procedure that has already been used by Cheng [54]. We note that Biswas and Manna [55] have previously reported the existence of these same flow patterns that originate in a bottom-heated square cavity filled with air, where both the cooled (or adiabatic) sidewalls are translating at a constant velocity in their own planes either vertically upward or vertically downward, while the top wall is considered either adiabatic or maintained at a cold constant temperature.

(a)

Ri=35.3   Ri=2.78   Ri=12.86

(b)

Ri=62.87   Ri=0.98   Ri=15.35

(c)

Ri=25.18   Ri=0.2   Ri=11.35

Fig. 7. Contours of streamlines (first row), isotherms (second row) for different Richardson numbers (Ri) at (a) Pr=2.0, (b) Pr=3.0454 and, (c) Pr=5.534
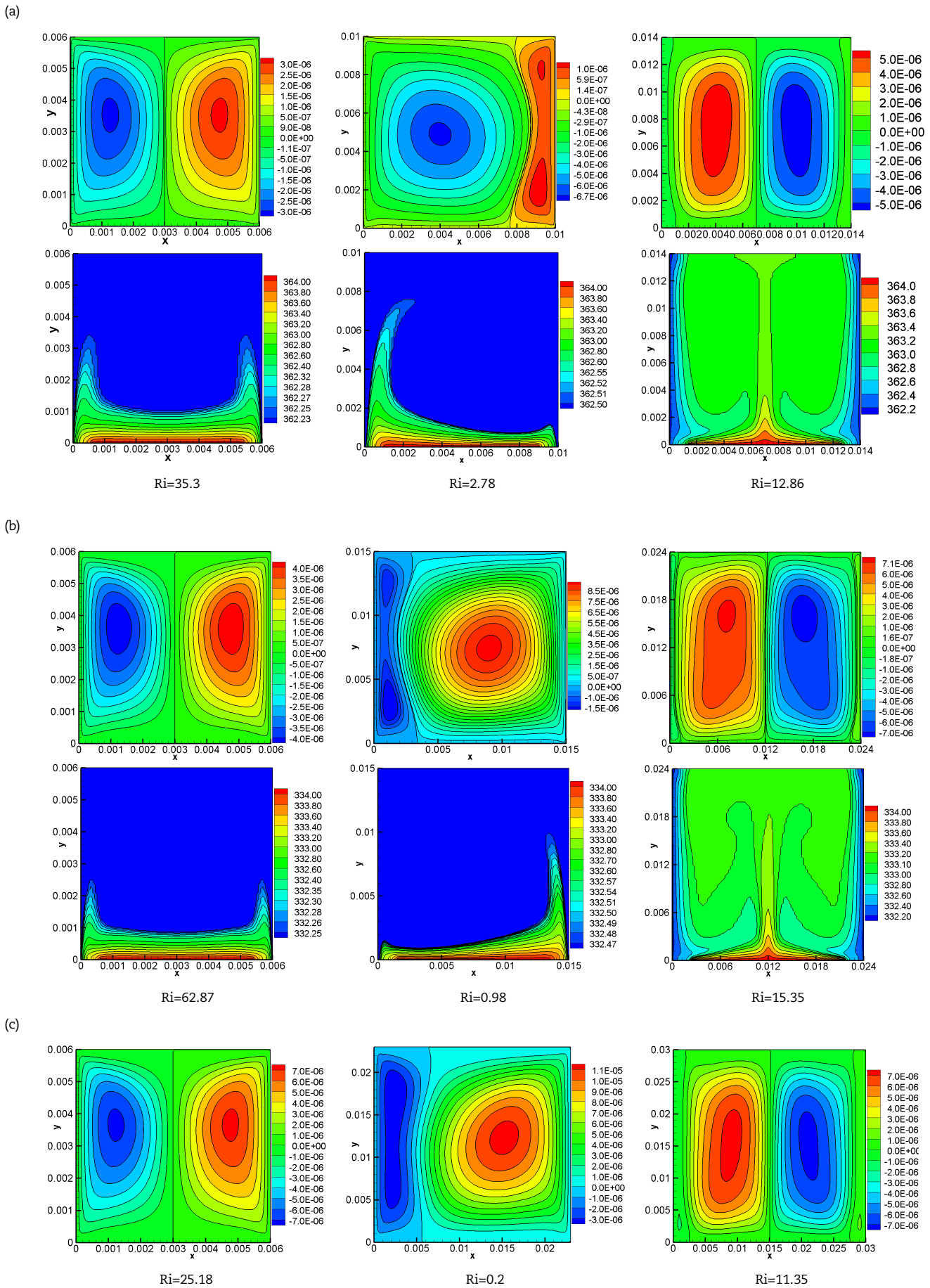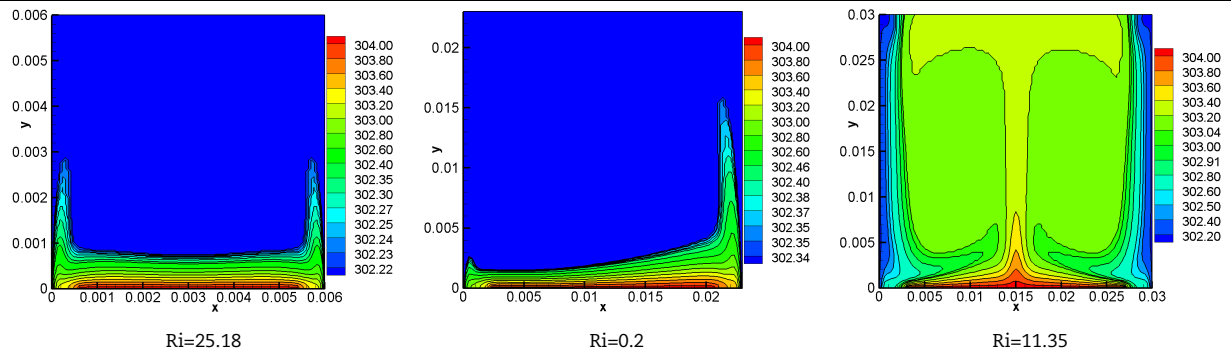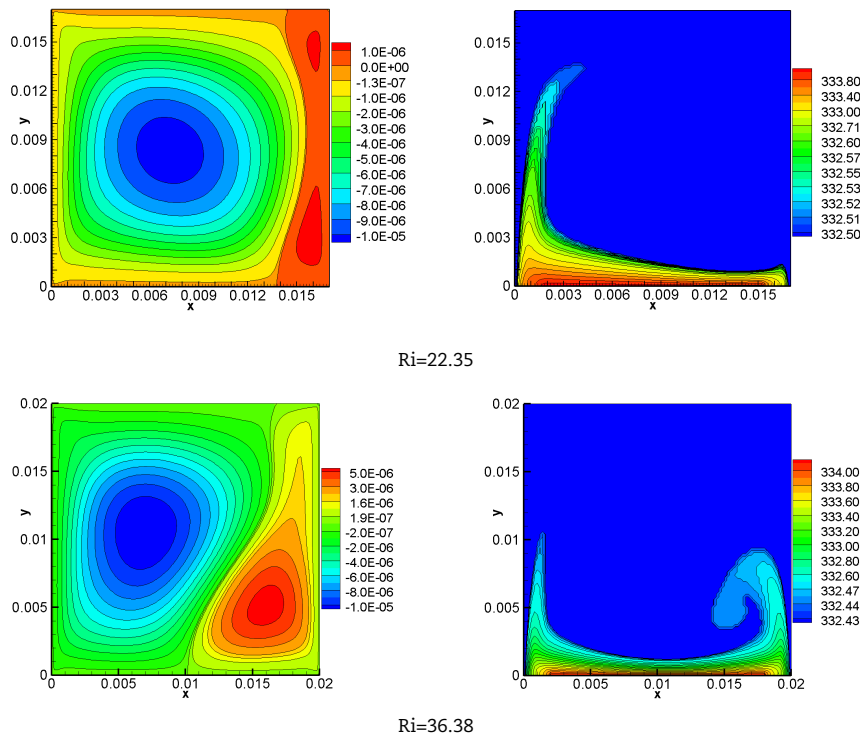
Fig. 7. Contours of streamlines (first row), isotherms (second row) for different Richardson numbers (Ri) at (a) Pr=2.0, (b) Pr=3.0454 and, (c) Pr=5.534

Fig. 8. Comparison of streamlines (left column) and isotherms (right column) for Ri=22.35 and, 35.36 at Pr= 3.045

If this figure reveal that the dynamic and thermal fields show the same trend with the variation of the Richardson number (Ri) i.e. by highlighting the three types of fluid flow previously described, however, it was observed that for Pr = 3.045 and Ri between 22.35 (L = 0.017 m) and 36.38 (L = 0.02m) the distributions of streamlines and temperature contours are considerably altered and another interesting type of fluid flow appears. To better identify and define this unexpected and disconcerting new type of flow regime, the main characteristics of streamlines and isotherms in the cavity for the Richardson number limit values cited above are compared in Fig. 8. The figure indicates that for Ri = 22.35 the streamlines displayed consist of two strictly antisymmetric cells with respect to the vertical median axis (x =L / 2) but are practically symmetrical with respect to the horizontal median axis (y = L / 2). We also note that the heat from the hot source spreads on one of the side walls only. However, for Ri = 36.38, the new type of flow regime is characterized by two non-symmetrical cells, not only with respect to the vertical median axis (x=L/2) but also with respect to the horizontal median axis (y= L/2). On the other hand, unlike the case earlier the isotherms propagate along the two sidewalls of the cavity. It is also important to point out that when the new type of flow is considered, the behavior of the flow is often unpredictable. To illustrate this point, a comparison of the average Nusselt number for Ri=22.35 and 36.38 is showed in Fig. 9. We can see that, for Ri = 22.35, the evolution of the mean value of the Nusselt number converges to a fixed value, while for Ri = 36.38 the evolution of the same number remains so fluctuating that no exact value cannot be practically determined. It should be noted also that this instability and complexity of the fluid flow and the heat transfer have been verified and validated experimentally by Sukhanovsky, and Evgrafova [56, 57] by examining closely, laminar and transient convective regimes from localized heat source inside a silicon oil-filled cylindrical vessel of different diameters at different values of Prandtl number (Pr = 209, 104, 67, and 38) at T = 25°C.

Furthermore, a similar trend is observed when the flow progresses from the new type of flow regime (two non-symmetrical cells) to the third type of flow regime (four symmetric cells). Here, too, we noted, from Fig. 10 (a), that the evolution of the average Nusselt number at Pr=3.045 for Ri=62.87, characterizing the third type of flow regime (four symmetric cells) develops also unpredictable fluctuations which begin to amplify when the time exceeds 900 s. By contrast, for the other Prandtl numbers (Pr=2. and Pr=5.534) the fluid flow remains always stable for the same type of flow regime (four symmetric cells). Figure 10(b) has been used to visualize this stability at arbitrary values of the Richardson numbers characterizing the same type of flow regime (four symmetric cells). It should be noted that the evolution of the average Nusselt number for Pr=2.0 at Ri=35.3, as it is for Pr=5.534 at Ri = 25.18, evolves towards a constant value showing a stable development of the fluid flow.
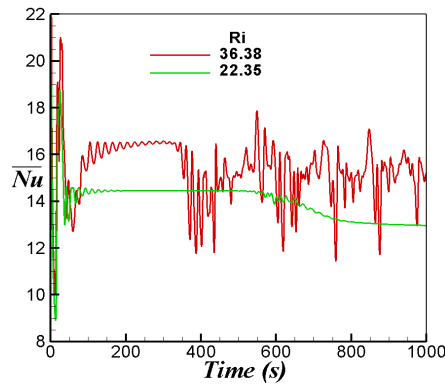
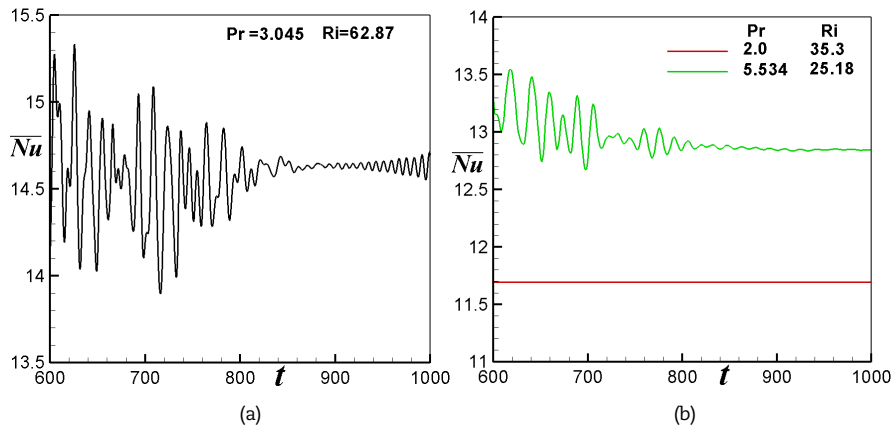**Fig. 9.** Comparison of the average Nusselt number $\overline{Nu}$ for Ri=36.38 and, 22.35 at Pr= 3.045

Fig. 10. Comparison of the evolution of the average Nusselt number (a) for Pr= 3.045 at Ri= 62.87; (b) for Pr=2.0, and, 5.534 at Ri=35.3 and, 25.18, respectively

Finally, we have briefly summarized in Table 3, the identification of the different types of flow regimes, defined by their Richardson numbers (Ri) and the corresponding length of the cavity (L), for the Prandtl numbers (Pr) considered in this study.

Having set out results of local distributions through temperature fields, and flow fields, in the following section we will present results of the heat transfer rate, which is characterized by the Nusselt number.

4.2 Heat transfer rate

The heat transferred from the hot source can be measured by the average Nusselt number. The effect of the Richardson number on the evolution of the average Nusselt number for the cases of Pr=2.0, 3.045, and 5.534 is shown in Fig. 11. It is to be noted that the same values of Ri that characterize the structure of streamlines and isotherms, previously presented, have been taken into account to represent the evolution of the average Nusselt number for each type of flow regime. In general, we noted that the average Nusselt number, whatever the Prandtl number, exhibits fluctuations at the beginning that are becoming increasingly important as the Richardson number increases before stabilizing at a fixed value. Furthermore, the regime with two non-symmetrical cells is characterized by a sudden drop in the evolution of the mean Nusselt number. It can be seen also that the more Ri increases, whatever the Prandtl number, the more heat is transferred from the heated bottom wall, either along sidewalls (the first and the second type of flow regime) or along the central part of the cavity (the third type of flow regime). It means that the temperature gradient at the heated bottom wall also increases and consequently the Nusselt number is achieving increased significance. On the other hand the computational times for which flows become steady increase as the Richardson and Prandtl numbers increase simultaneously and, their approximate values are 600 s, 1000 s, and 5000 s at Pr=2.0, 3.045, 5.534 respectively. In other words, the steady-state is reached more quickly when the Prandtl number decreases. It is rightly noted that in the case of Pr = 5.545 a computational time of between 2 and 3 days, on an "HP Z820 Workstation", is required for each numerical simulation to ensure the stability of the fluid flow when the Richardson number is between 11.35 (L=0.02m) and 18.36 (L=0.03m).

Table 3. Identification of the different types of flow regimes for the Prandtl numbers considered.

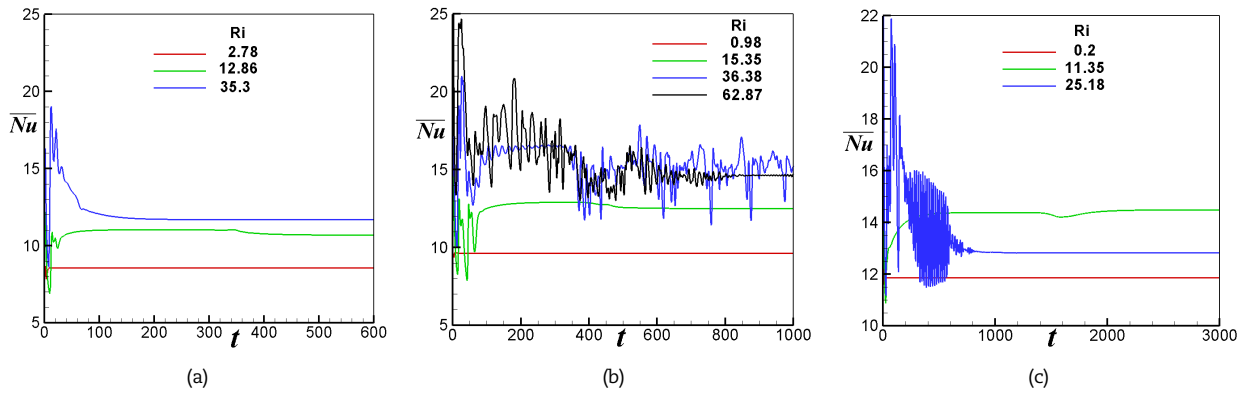| Flow regime	First Type	Second type	Third type
Pr=2.0 stable	$0.823 \leq Ri \leq 4.41$ $0.004 \leq L \leq 0.007$	$6.58 \leq Ri \leq 19.56$ $0.008 \leq L \leq 0.0115$	$Ri \geq 22.22$ $L \geq 0.012$
Pr=3.045 stable	$0.291 \leq Ri \leq 6.06$ $0.004 \leq L \leq 0.011$	$6.92 \leq Ri \leq 22.34$ $0.0115 \leq L \leq 0.017$	------------
Pr=3.045 unstable	----------------------	$26.52 \leq Ri \leq 36.38$ $0.018 \leq L \leq 0.023$	$Ri \geq 48.43$ $L \geq 0.024$
Pr=5.534 stable	$0.0597 \leq Ri \leq 9.93$ $0.004 \leq L \leq 0.022$	$11.35 \leq Ri \leq 18.36$ $0.023 \leq L \leq 0.027$	$Ri \geq 20.47$ $L \geq 0.28$

Fig. 11. Time series of the average Nusselt number $\overline{Nu}$ for different Ri, (a) Pr=2.0, (b) Pr=3.045 and, (c) Pr=5.534
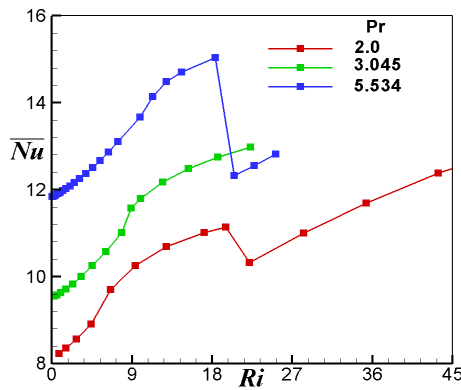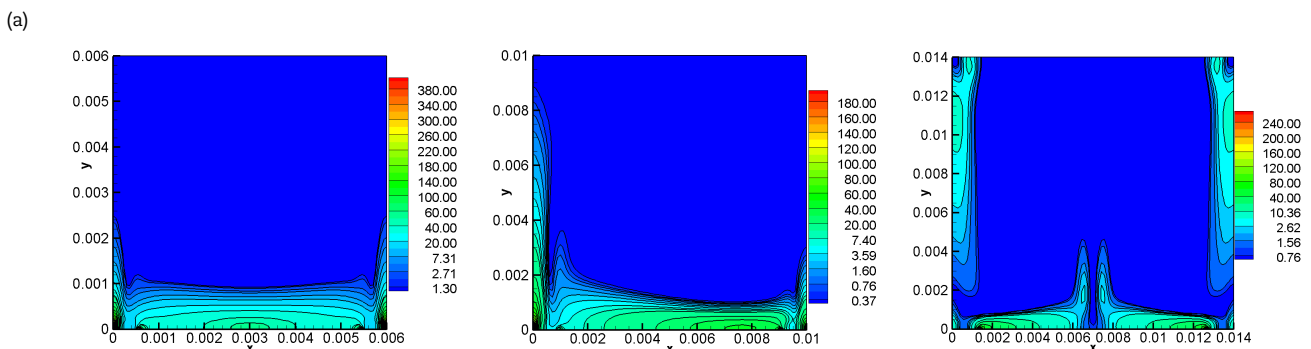

Fig. 12. Comparison of the average Nusselt number ($\overline{Nu}$) as a function of the Richardson number (Ri) for the considered values of Prandtl number (Pr)

Figure 12 demonstrates the comparison of the average Nusselt number as a function of the Richardson number for the three Prandtl numbers considered (2.0, 3.045 and, 5.534). It is easily visible that an increase in the value of the Prandtl number (i.e. a decrease in the temperature of the heat source) leads to a significant enhancement in the average Nusselt. A fluid with a higher Prandtl number has a relatively lower thermal diffusivity (see table 1), which reduces heat conduction and thereby increases the temperature gradient at the heated surface and consequently may also significantly increase the average Nusselt number [58]. However, a comparison of the average Nusselt number at Pr=2.0 and 5.534, clearly indicates that the transition from the second type of flow (two unsymmetrical cells) to the third one (four symmetric cells), is evidenced by a sudden drop in the average Nusselt number (second bifurcation). This does not apply to the particular case where Pr=3.045 because we have already seen that the solution becomes so unstable that it becomes impossible, starting from Ri=26.52, to obtain reliable fair values for the different fundamental unknowns of the problem.

4.3 Characteristics of entropy generation

The contours of the total entropy generation (first row), and entropy generation due to fluid friction (second row), for the same Richardson numbers previously considered, at the Prandtl numbers of 2.0, 3.045, and 5.534 are presented in Fig. 13 a, b and, c respectively. In most of the cases entropy production is more pronounced at the walls and less at the core region of the cavity. Moreover, the contours of the total entropy generation occur strongly near the active part (i.e. the heated portion located on the bottom of the cavity) and progress rapidly along the sidewalls as the Richardson number increases. This is due to high-temperature gradients along the vertical direction. Also, this figure depict that the contours of the local entropy generation due to fluid friction are found to be significant only near the cold sidewalls and in the corners but becomes negligible at the core of the cavity. In this particular case, the cause of the problem can mainly be attributed to the gradients of the vertical velocity component. By comparing the temperature contours in Fig. 7, a, b, c (second row) with those of the total entropy generation in Fig. 13, a ,b ,c (first row), and whatever the values of Richardson and Prandtl numbers, it can be seen that they appear to be sufficiently similar in both cases. This means that temperature gradients play an important role in the creation of entropy generation. A similar conclusion has been reported very recently (July 2021) by Khetib et al. [59].
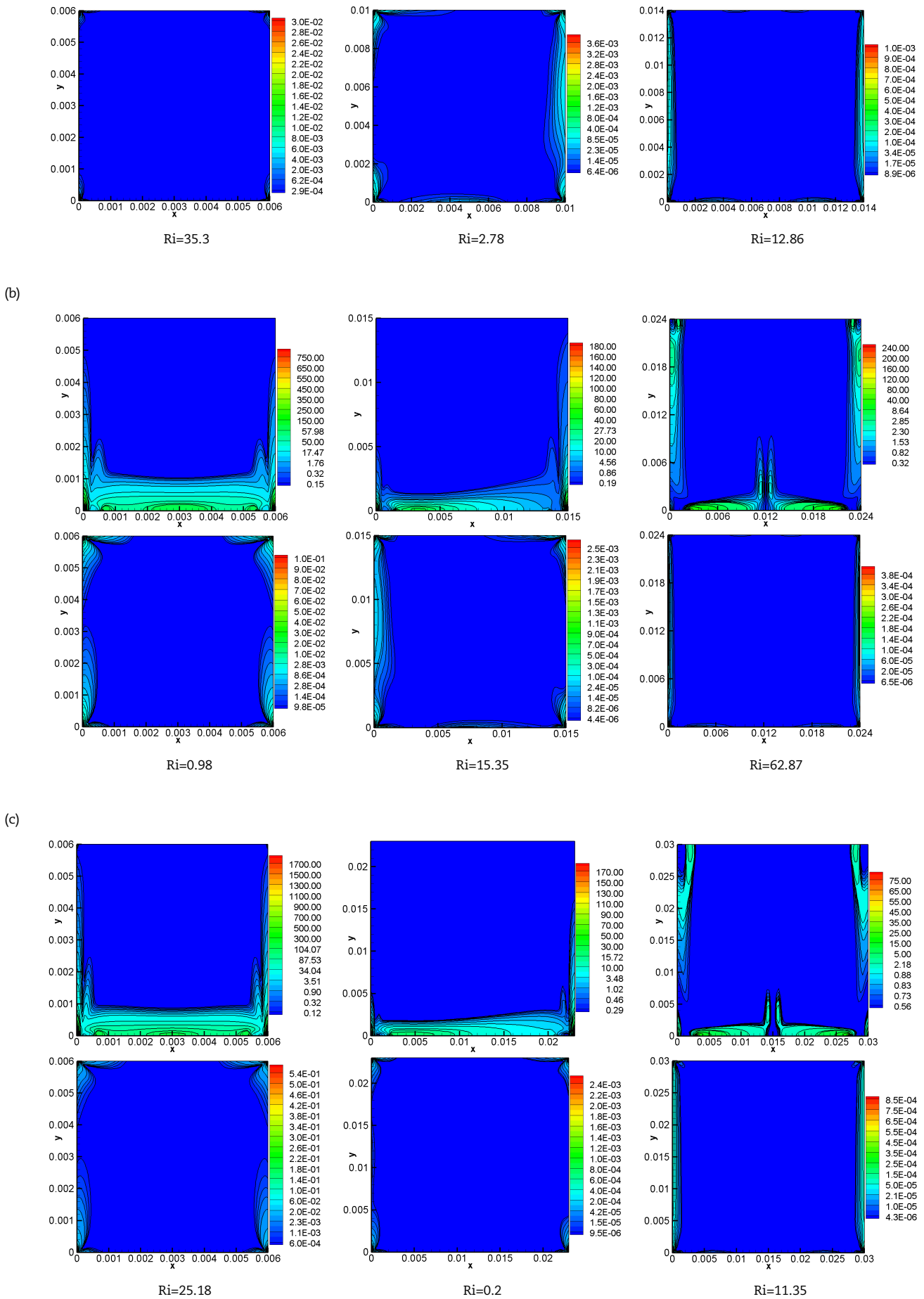
(a)

Fig. 13. Contours of total entropy generation (first row), and entropy generation due to fluid friction (second row), for different Richardson numbers (Ri)) at (a) Pr=2.0, (b) Pr=3.0454 and, (c) Pr=5.534
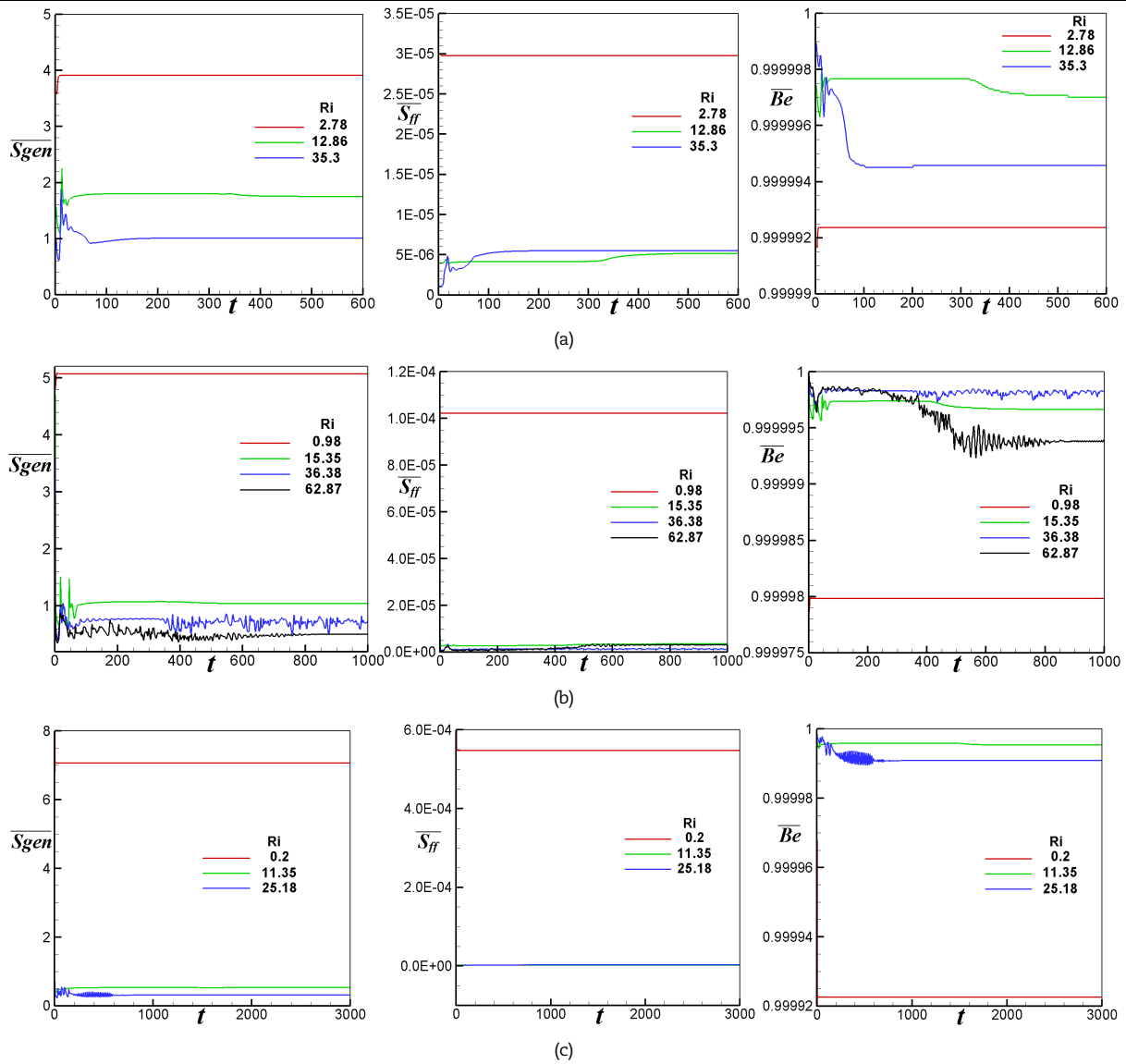
Fig. 14. Time traces of the average total entropy generation (first row), the average entropy generation due to fluid friction (second row) and the average Bejan number (third row), for different Richardson numbers (Ri)) at (a) Pr=2.0, (b) Pr=3.0454 and, (c) Pr=5.534
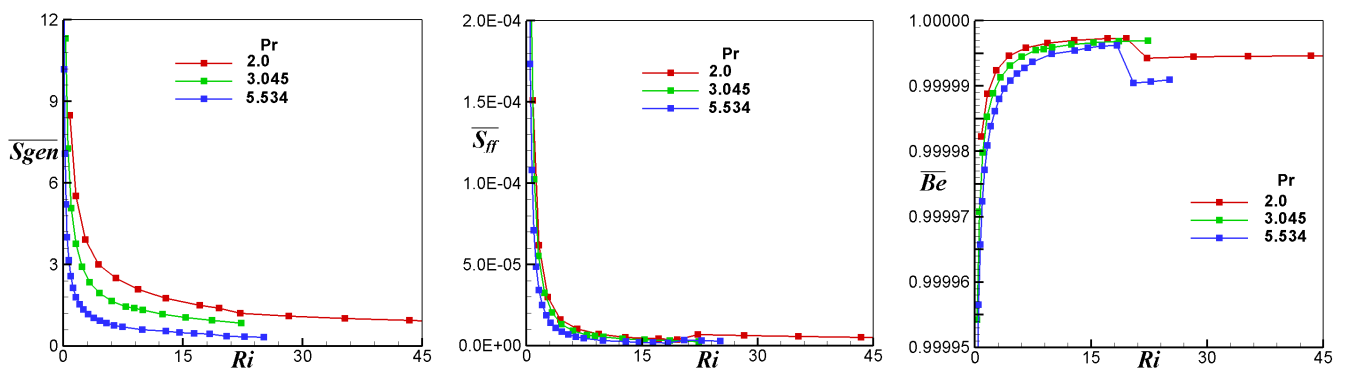

Fig. 15. Comparison of the average entropy generation, the average entropy generation due to fluid friction and, the average Bejan number vs. the Richardson number (Ri) for the considered values of Prandtl number (Pr)

On the other hand, a comparison of the scales of the values of the total entropy generation and that due to the fluid friction reveals that, irrespective of the Prandtl and Richardson numbers, entropy generation due to fluid friction is so insignificant that we can conclude, in accordance with equation (13) that the average Bejan number is very close to one. Hence, the trend of changes in the thermal entropy generation rate is similar to the total entropy generation rate. It was therefore decided, only in order to lighten the text, that the contours and, the profile of the average thermal entropy generation and, the contours of the Bejan number would not be included in this study.

The time traces of the average total entropy generation (first row), the average entropy generation due to fluid friction (second row) and, the average Bejan number (third row), for the same Richardson and Prandtl numbers, previously considered, are presented in Fig. 14 a, b and c). It should be noted that when the Richardson numbers increase, the total entropy production and the entropy generation due to fluid friction decrease while the Bejan number increases. Also, it is noted that the values of the average entropy generation due to fluid friction are insignificant in comparison to those of the average global entropy generation which implies that the average Bejan number is very close to 1.0.

Figure 15 shows the average entropy production $\overline{s_{gen}}$, the average entropy generation due to fluid friction $\overline{s_{ff}}$ and the average Bejan number $\overline{Be}$ of the system vs. the Richardson numbers, and illustrates the direct influence of the Prandtl numbers considered. It should be noted that when these Prandtl numbers increase, the total entropy production and the average entropy generation due to fluid friction decrease. The curves describe a similar behavior to that followed by the curves of the average Nusselt numbers, the only difference is, in this case, that when the Prandtl numbers increase, the average Nusselt numbers also increase.

5. Conclusion

The present numerical investigation examines the mixed convection in a water-filled square cavity partially heated from below. The impact of the Richardson and, Prandtl numbers on heat transfer, fluid flow, and entropy generation is analyzed and discussed. The obtained results can be synthesized as follow:

- The flow patterns and thermal field change significantly with the increase in the Richardson and Prandtl numbers. Indeed, the obtained results show that, irrespective of the Prandtl number, for low Ri the heat transfer and entropy generation patterns are symmetric, whereas with increasing Ri these patterns become asymmetric and more complex.
- Unstable flows appear for a Richardson number greater than or equal to 26.52 (L=0.18m) at Pr = 3.045.
- An increase in the Prandtl number, irrespective of the Richardson number, causes an increase in the average Nusselt number.
- For all cases, the entropy production decreases when both the Richardson and Prandtl numbers simultaneously increase.
- The average Bejan number is always close to one which reveals that the contribution of the thermal irreversibility to the total entropy generation is always much more important than the fluid friction irreversibility.

Author Contributions

S. Boudebous initiated and planned the project. H. Koten developed and formulated the mathematical model. N. Ferroudj developed the code, conducted the numerical experiments, and examined the validation of the result. Both authors contributed equally and significantly in writing this paper. All authors analyzed, discussed the results, reviewed and approved the final version of the manuscript.

Acknowledgments

Conflict of Interest

The authors declared no potential conflicts of interest with respect to the research, authorship, and publication of this article.

Funding

Data Availability Statements

The datasets generated and/or analyzed during the current study are available from the corresponding author on reasonable request.

Nomenclature

Be	Bejan number	**Greek Symbols**	
g	Gravitational acceleration [ms-2]		
Gr	Grashof number (= $g\beta\Delta TL^3/\nu^2$)	α	Thermal diffusivity, [$m^2\ s^{-1}$]
k	Thermal conductivity [$Wm^{-1}\ K^{-1}$]	β	Thermal expansion coefficient, [K^{-1}]
l	heat source Length [m]	ΔT	Temperature difference (=Th -Tc), [K]
L	Length of the square cavity [m]	ν	Kinematic viscosity, [$m^2\ s^{-1}$]
Nu	Nusselt number	μ	Dynamic viscosity, [$kg\ m^{-1}s^{-1}$]
Pr	Prandtl number, (= ν/α)	ρ	Density, [$kg\ m^{-3}$]
Re	Reynolds number, (=$v_w L/\nu$)	ψ	Stream function, [$m^2.s^{-1}$]
Ri	Richardson number, (Gr/Re²)	ω	Vorticity, [s^{-1}]
Sgen	Local entropy generation [$Wm^{-3}K^{-1}$]		
t	Time [s]	**Subscripts**	
T	Absolute temperature [K]		
T_0	Bulk temperature (=Th +Tc)/2) [K]	C	Cold
u,v	Velocity components in x, y directions [$m\ s^{-1}$]	H	Hot
v_w	Side wall velocity (= νRe/L) [$m\ s^{-1}$]	ff	Fluid friction
x, y	Dimensional Cartesian coordinates [m]	Th	Thermal

References

[1] Ait Hssain, M., Mir, R., and El Hammami, Y., Numerical Simulation of the Cooling of Heated Electronic Blocks in Horizontal Channel by Mixed Convection of Nanofluids, *Journal of Nanomaterials*, 2020, Article ID 4187074, 11 p.

[2] Vasiliev, A. Yu., Sukhanovskii, A. N., Stepanov, R. A., Convective turbulence in a cubic cavity under nonuniform heating of a lower boundary, *Journal of Applied Mechanics and Technical Physics*, 61, 2020, 1049-1058.

[3] Dhahad, H.A., Al-Sumaily, G.F., Habeeb, L.J., Thompson, M.C., The Cooling Performance of Mixed Convection in a Ventilated Enclosure With Different Ports Configurations, *Journal of Heat Transfer*, 142(12), 2020, 122601.

[4] Vasiliev, A., Sukhanovskii, A., Turbulent convection in a cube with mixed thermal boundary conditions: low Rayleigh number regime, *International Journal of Heat and Mass Transfer*, 174, 2021, 121290.

[5] Hu, Z.X., Cui, G.X., Zhang, Z.S., Numerical study of mixed convective heat transfer coefficients for building cluster, *Journal of Wind Engineering and Industrial Aerodynamics*, 172, 2018, 170-180.

[6] Sheikholeslami, M., Farshad, S.A., Shafee, A., Babazadeh, H., Performance of solar collector with turbulator involving nanomaterial turbulent regime, *Renewable Energy*, 163, 2021, 1222-1237.

[7] Kumar, A., Ray, R.K., Sheremet, M.A., Entropy generation on double-diffusive MHD slip flow of nanofluid over a rotating disk with nonlinear mixed convection and Arrhenius activation energy, *Indian Journal of Physics*, 2021, doi: 10.1007/s12648-021-02015-2.

[8] Youcef , A., Saim, R., Numerical Analysis of the Baffles Inclination on Fluid Behavior in a Shell and Tube Heat Exchanger, *Journal of Applied and Computational Mechanics*, 7, 2021, 312-320.

[9] Ghalambaz, M., Jun Zhang, J., Conjugate solid-liquid phase change heat transfer in heatsink filled with phase change material-metal foam, *International Journal of Heat and Mass Transfer*, 146, 2020, 118832.

[10] Ghalambaz, M., Mehryan, S.A.M., Hajjar, A, Veismoradi, A., Unsteady natural convection flow of a suspension comprising Nano-Encapsulated Phase Change Materials (NEPCMs) in a porous medium, *Advanced Powder Technology*, 31(3), 2020, 954-966.

[11] Hajjar, A., Mehryan, S.A.M., Ghalambaz, M., Time periodic natural convection heat transfer in a Nano-encapsulated phase-change suspension, *International Journal of Mechanical Sciences*, 166, 2020, 105243.

[12] Ghalambaz, M., Zadeh, S. M. H., Mehryan, S.A.M., Pop, I., Wen, D.S., Analysis of melting behavior of PCMs in a cavity subject to a non-uniform magnetic field using a moving grid technique, *Applied Mathematical Modelling*, 77(2), 2020, 1936-1953.

[13] Bejan, A., A study of entropy generation in fundamental convective heat transfer, *Journal of Heat Transfer*, 101(4), 1979, 718-725.

[14] Bejan, A., The thermodynamic design of heat and mass transfer processes and devices, *Journal of Heat and Fluid Flow*, 8, 1987, 258-275,

[15] Izadi, S., Armaghani, T., Ghasemiasl, R., Chamkha, A.J., Molana, M., A comprehensive review on mixed convection of nanofluids in various shapes of enclosures, *Powder Technology*, 343, 2019, 880–907.

[16] Mustafa Abdul Salam, M., Hasanen Mohammed, H., Auday Awad, A., Laith Jaafar, H., Review on Mixed Convective Heat Transfer in Different Geometries of Cavity with Lid Driven, *Journal of Mechanical Engineering Research and Developments*, 43(7), 2020, 12-25.

[17] Yang, L., Kai Du, K., A comprehensive review on the natural, forced, and mixed convection of non-Newtonian fluids (nanofluids) inside different cavities, *Journal of Thermal Analysis and Calorimetry*, 140, 2020, 2033–2054.

[18] Oztop, H.F., Al-Salem, K., A review on entropy generation in natural and mixed convection heat transfer for energy systems, *Renewable and Sustainable Energy Reviews*, 16(1), 2012, 911–920.

[19] Sciacovelli, A., Verda, V., Sciubba, E, Entropy generation analysis as a design tool-a review, *Renewable & Sustainable Energy Reviews*, 43, 2015, 1167–1181.

[20] Biswal, P., Basak T., Entropy generation vs energy efficiency for natural convection based energy flow in enclosures and various applications: A review, *Renewable & Sustainable Energy Reviews*, 80, 2017, 1412-1457.

[21] Sheikholeslami, M., Arabkoohsar, A., Ismail, K.A.R., Entropy analysis for a nanofluid within a porous media with magnetic force impact using non-Darcy model, *International Communications in Heat and Mass Transfer*, 112, 2020, 104488.

[22] Sheikholeslami, M., Farshad, S.A., Shafee, A., Babazadeh H., Numerical modeling for nanomaterial behavior in a solar unit analyzing entropy generation, *Journal of the Taiwan Institute of Chemical Engineers*, 112, 2020, 271-285.

[23] Selimefendigil, F., Öztop, H.F., Sheikholeslami, M., Impact of local elasticity and inner rotating circular cylinder on the magneto-hydrodynamics forced convection and entropy generation of nanofluid in a U-shaped vented cavity, *Mathematical Methods in the Applied Sciences*, 2020, doi: 10.1002/mma.6930.

[24] Rabbi, K.Md., Sheikholeslami, M., Karim, A., Shafee, A., Li, Z., Tlili, I., Prediction of MHD flow and entropy generation by Artificial Neural Network in square cavity with heater-sink for nanomaterial, *Physica A: Statistical Mechanics and its Applications*, 541(1), 2020, 123520.

[25] Mondal, P., Mahapatra, T.R., Parveen, R., Entropy generation in nanofluid flow due to double diffusive MHD mixed convection, *Heliyon*, 7, 2021, e06143.

[26] Ebrahimi, D., Yousefzadeh, S., Akbari, O.A., Montazerifar, F., Rozati, S.A., Nakhjavani, S., Safaei, M.R., Mixed convection heat transfer of a nanofluid in a closed elbow⊠shaped cavity (CESC), *Journal of Thermal Analysis and Calorimetry*, 2021, doi: 10.1007/s10973-021-10548-1.

[27] Khosravi, R., Rabiei, S., Khaki, M., Safaei, M.R., Goodarzi, M., Entropy generation of graphene-platinum hybrid nanofluid flow through a wavy cylindrical microchannel solar receiver by using neural networks, *Journal of Thermal Analysis and Calorimetry*, 2021, doi: 10.1007/s10973-021-10828-w.

[28] Cimpean, D.S. and Pop, I. (2021), Entropy generation of a nanofluid in a porous cavity with sinusoidal temperature at the walls and a heat source bellow, *International Journal of Numerical Methods for Heat & Fluid Flow*, 2021, doi: 10.1108/HFF-10-2020-0654.

[29] Maougal, A., Bessaih, R., Heat Transfer and Entropy Analysis for Mixed Convection in a Discretely Heated Porous Square Cavity, *Fluid Dynamics & Materials Processing*, 9(1), 2013, 35-59.

[30] Roy, M., Roy, S., Basak, T., Analysis of entropy generation on mixed convection in square enclosures for various horizontal or vertical moving wall(s), *International Communications in Heat and Mass Transfer*, 68, 2015, 258-266.

[31] Roy, M., Basak, T., Roy, S., Pop, I., Analysis of Entropy Generation for Mixed Convection in a Square Cavity for Various Thermal Boundary Conditions, *Numerical Heat Transfer, Part A: Applications*, 68(1), 2015, 44-74

[32] Roy, M., Basak, T., Roy, S., Analysis of Entropy Generation During Mixed Convection in Porous Square Cavities: Effect of Thermal Boundary Conditions, *Numerical Heat Transfer, Part A*, 68, 2015, 925–957.

[33] Roy, M., Biswal, P., Roy, S., Basak, T., Role of various moving walls on entropy generation during mixed convection within entrapped porous triangular cavities, *Numerical Heat Transfer, Part A: Applications*, 71(4), 2017, 423-447.

[34] Bhatti, M.M., Ali Abbas, M., Rashidi, M., Entropy Generation in Blood Flow With Heat and Mass Transfer for the Ellis Fluid Model, *Heat Transfer Research*, 49(8), 2018, 747-760.

[35] Bhatti, M.M., Sheikholeslami, M., Shahid, A., Hassan, M., Abbas, T., Entropy generation on the interaction of nanoparticles over a stretched surface with thermal radiation, *Colloids and Surfaces A: Physicochemical and Engineering Aspects*, 570(5), 2019, 368-376.

[36] Khan,I., Khan, W.A., Qasim, M., Idrees Afridi, A., Sayer O. Alharbi, S.O., Thermodynamic Analysis of Entropy Generation Minimization in Thermally Dissipating Flow Over a Thin Needle Moving in a Parallel Free Stream of Two Newtonian Fluids, *Entropy*, 21(1), 2019, 74.

[37] Öⵇüt, E.B., Second Law Analysis of Mixed Convection of Magneto hydrodynamic Flow in an Inclined Square Lid-Driven Enclosure, *Journal of Thermal Engineering*, 5(6), 2019, 240-251.

[38] Mehta, S.K., Pati, S., Numerical study of thermo-hydraulic characteristics for forced convective flow through wavy channel at different Prandtl numbers, *Journal of Thermal Analysis and Calorimetry*, 141, 2020, 2429–2451.

[39] Kashyap, D., Dass, A.K., Oztop, H.F., Abu-Hamdeh, N., Multiple-relaxation-time lattice Boltzmann analysis of entropy generation in a hot-block-inserted square cavity for different Prandtl numbers, *International Journal of Thermal Sciences*, 165, 2021, 106948.

[40] Sahaya Jenifer, A., Saikrishnan, P., Lewis, R.W., Unsteady MHD Mixed Convection Flow of Water over a Sphere with Mass Transfer, *J. Appl. Comput. Mech.*, 7(2), 2021, 935-943.

[41] Abanoub, G. K., Eman H. H., Sarwat N. H., Numerical simulation of three-sided lid-driven square cavity, *Engineering Reports*, 2, 2020, e12151.

[42] Bejan, A., *Entropy Generation Through Heat and Fluid Flow*, First Edition, Willey & Sons, 1982.

[43] Micula, S., Pop, I, Numerical results for the classical free convection flow problem in a square porous cavity using spline functions. *Int. J. Numer. Methods Heat Fluid Flow*, 31(3), 2021, 753–765.

[44] Kawamura, T., Takami, H., Kuwahara, K., New higher order upwind scheme for incompressible Navier-Stokes equations. Ninth International

Conference on Numerical Methods in Fluid Dynamics. *Lecture Notes in Physics*, 1985, 218, 291-295.

[45] Bejan, A., *Heat Transfer*, Wiley, New York, 1993

[46] Dinçer, I., Zamfirescu, C., *Dring Phenomena: Theory and Applications*, First Edition, John Wiley & Sons, 2016.

[47] Ferziger, J.H., and M. Peric, M., *Computational Methods for Fluid Dynamics,* Springer, 2002.

[48] Pallares, J., Arroyo, M.P., Grau, F.X., and, Giralt F., Experimental laminar Rayleigh-Benard convection in a cubical cavity at moderate Rayleigh and Prandtl numbers, *Experiments in Fluids*, 31(2), 1998, 208–218.

[49] Goodarzi, M., Safaei, M. R, Oztop, H. F., Karimipour, A., Sadeghinezhad, E, Dahari, M., Kazi, S. N. and Jomhari1, N., Numerical Study of Entropy Generation due to Coupled Laminar and Turbulent Mixed Convection and Thermal Radiation in an Enclosure Filled with a Semitransparent Medium, *The Scientific World Journal*, Article ID 761745, 2014, 8 p.

[50] Patil, P.M, Latha, D.N., Chamkha, A.J., Non-similar Solutions of MHD Mixed Convection over an Exponentially Stretching Surface: Influence of Non-uniform Heat Source or Sink, *J. Appl. Comput. Mech.*, 7(3), 2021, 1334-1347.

[51] Asad, M.F.A. , Nur Alam, M., Tunç, C., Sarker., M.M.A., Heat Transport Exploration of Free Convection Flow inside Enclosure Having Vertical Wavy Walls, *J. Appl. Comput. Mech.*, 7(2), 2021, 520-527.

[52] Jani, S., Mahmoodi, M., Amini, M., Magnetohydrodynamic Free Convection in a Square Cavity Heated from Below and Cooled from Other Walls, *International Journal of Mechanical and Mechatronics Engineering*, 7(4), 2013,750-755.

[53] Aydin, O., Yang, W. J., Mixed convection in cavities with a locally heated lower wall and moving sidewalls, *Numerical Heat Transfer Part A*, 37, 2000, 695-710.

[54] Cheng, T.S., Characteristics of mixed convection heat transfer in a lid-driven square cavity with various Richardson and Prandtl numbers, *International Journal of Thermal Sciences*, 50(2), 2011, 197-205.

[55] Biswas, N., Manna, N.K., Transport phenomena in a sidewall-moving bottom-heated cavity using heatlines, *Sādhanā*, 42(2), 2017, 193–211.

[56] Evgrafova, A., Sukhanovskii, A., Specifics of heat flux from localized heater in a cylindrical layer, *International Journal of Heat and Mass Transfer*, 135, 2019, 761-768.

[57]] Evgrafova, A., Sukhanovskii, A., Dependence of boundary layer thickness on layer height for extended localised heaters, *Experimental Thermal and Fluid Science*, 121, 2021, 110275.

[58] Nadeem, S., Khan, A.U., Saleem S., A comparative analysis on different nanofluid models for the oscillatory stagnation point flow, *Eur. Phys. J. Plus*, 131, 2016, 261.

[59] Khetib, Y., Alahmadi, A.A., Alzaed, A., Azimy, H., Sharifpur, M., Cheraghian, G., Effect of Straight, Inclined and Curved Fins on Natural Convection and Entropy Generation of a Nanofluid in a Square Cavity Influenced by a Magnetic Field, *Processes*, 9(8), 2021, 1339.

ORCID iD

Nawal Ferroudj https://orcid.org/0000-0001-7743-0971
Hasan Koten https://orcid.org/0000-0002-1907-9420
Saadoun Boudebous https://orcid.org/0000-0003-0136-0748

Publisher's Note Shahid Chamran University of Ahvaz remains neutral with regard to jurisdictional claims in published maps and institutional affiliations.